

Controllable Antibacterial Activity through Acid-Triggered Molecular Cage Release of Stored Ag⁺

Wencheng Zhu ^{[b].1}, Haitao Yu ^{[a,c].1}, Yanju Luo ^[d], Shunwei Chen ^{[a].*}, Xujun Zheng ^{[e].*}

^a School of Materials Science and Engineering, Qilu University of Technology (Shandong Academy of Sciences), Jinan 250303, China

^b Institute of Neuroscience, CAS Center for Excellence in Brain Science and Intelligence Technology, Chinese Academy of Sciences, Shanghai 200031, China

^c School of Chemistry and Molecular Engineering, East China Normal University, Shanghai 200241, China

^d Analytical & Testing Center, Sichuan University, Chengdu 610064, China

^e Department of Chemistry, Duke University Durham, North Carolina 27708, United States

¹ These authors contributed equally to this work.

E-mail addresses: swchen@qlu.edu.cn (S.C.), xujun.zheng@duke.edu (X.Z.).

ABSTRACT:

Aiming for solving the emergence of drug-resistant bacteria worldwide, the construction of novel supramolecular self-assembly systems with antibacterial functions is attracting growing research attention. Herein, using dynamically reversible Schiff-base imine bonds as the assembly strategy, a three-dimensional pure organic cage, namely **4-cage**, was obtained in high yield. By taking advantage of the bidentate chelating capability of its imine-based skeleton, **4-cage** was demonstrated to serve as an Ag⁺-carrier. Owing to the acid-induced decomposition of this skeleton, the Ag⁺-loaded **4-cage** can controllably release Ag⁺ through pH regulation, hence, as a proof-of-concept, it is proved to be applicable as a controllable release antibacterial reagent. Such pH-responsive Ag⁺-carried supramolecular architecture may shed light on the molecule design strategies for bacterial elimination in different environments, or for controllable functions in various other fields.

Keywords: organic imine cage; Ag⁺; antibacterial; controllable release; pH-responsive.

1. Introduction

Bacteria widely exist in diverse environments, such as soil, ocean, and living organisms.¹ While some bacteria are demonstrated to be beneficial (e.g., Lactobacilli are probiotics that can ferment carbohydrates into lactic acid; methanotroph can

decompose trichloroethylene, tetrachloroethylene, and other organic pollutants), most of them are harmful. In fact, pathogenic bacterial infection is currently a major cause of human death and diseases.² Therefore, numerous efforts have been devoted to the development of antibacterial reagents. Among them, silver(I) ion is one of the most commonly used effective agents due to its combined broad-spectrum antimicrobial activity and low drug resistance risk.³ At present, Ag⁺-based antibacterial reagents have been extensively used in commercial and medical products (e.g., catheters, burn wound dressings, and dental implants),⁴⁻⁵ yet the dose-dependent cytotoxicity, as well as the accumulation risk of Ag⁺ ion inside the living organisms, have greatly hampered their further applications. Although these problems, in principle, could be resolved if the Ag⁺ concentration of these reagents could be delicately controlled under certain environments, so far, such controllable Ag⁺-based antibacterial systems are largely relied on nanoparticles.⁶ Developing novel strategies should provide alternative options that might be suitable for more potential applications.

Self-assembly has emerged as a powerful tool for the construction of diverse fascinating topologies ranging from basic zero-dimensional (0D) nanoparticles to two-dimensional (2D) macrocycles and frameworks, and even to three-dimensional (3D) cages and aggregates. These supramolecular assemblies have been demonstrated to be extraordinary versatile materials in gas adsorption/separation,⁷⁻⁸ ion/molecular recognition,⁹ catalysis,¹⁰⁻¹¹ sensing,¹² electroluminescence,¹³ cell imaging,¹⁴ and many other fields,¹⁵⁻¹⁹ by taking advantage of the highly tunable and dynamic nature of the noncovalent interactions. However, although supramolecular self-assembly has an inbuilt advantage over its covalent-bonded counterpart in constructing controllable drug-release systems, concerning active materials for antibacterial therapies,^{6, 20-26} hitherto no relevant reports could be found.

Herein, we present our findings that by borrowing dynamically reversible and Ag⁺-chelatable Schiff-base bond (also called imine bond, —C=N—) as the assembly strategy, a 3D pure organic cage (namely, **4-cage**) that is capable of storing Ag⁺ and then releasing it in certain pH environments is acquired. To the best of our knowledge, this is the first report on Ag⁺-preloaded self-assemblies that can stimulatingly release Ag⁺ for controllable antibacterial treatments. The proposed pH-responsive silver-carrying supramolecular cage shows great promise for antibacterial applications especially in acidic microenvironments, such as the living sites of acid-producing bacteria and bacterial infected sites in wounds and even tumors.²⁷⁻²⁹

2. Results and Discussion

To validate that the building block cyclohexanediamine or its bidentate Schiff-base derivative is a chelating ligand scaffold that could act as the binding sites for Ag^+ , initially, a structurally simple enamine molecule **Model** (Figure 1, Scheme S1 and Figures S1-S3) was synthesized through facile condensation between benzaldehyde (**Ph-CHO**) and (1*S*,2*S*)-(+)-1,2-diaminocyclohexane (**CHX-NH₂**). In addition, the **Model** can also provide indirect structural information on the coordination of Ag^+ with **4-cage**, since the combination between **4-cage** and Ag^+ will produce a precipitate (named as **Ag⁺@4-cage**) which makes it difficult to be characterized. The binding behavior of **Model** with Ag^+ was investigated in a mixed solvent system of $\text{CDCl}_3/\text{CD}_3\text{OD}$ via ^1H NMR. As shown in Figure 1b-1g, with increasing Ag^+ concentration (0→2.0 equiv.), although the NMR signal of most protons has nearly unaltered, both the imine $\text{H}_{\text{d}'}$ and cyclohexane $\text{H}_{\text{e}'}$ protons display a downfield-shifted effect, indicating the successful coordination of Ag^+ with **Model** at its imine site. This deduction was further confirmed by the electrospray ionization mass spectrometry (ESI-MS), where a signal peak at m/z 397.1 that corresponds to the molecular ion peak of the **Ag⁺@Model** complex was observed (Figure S4).

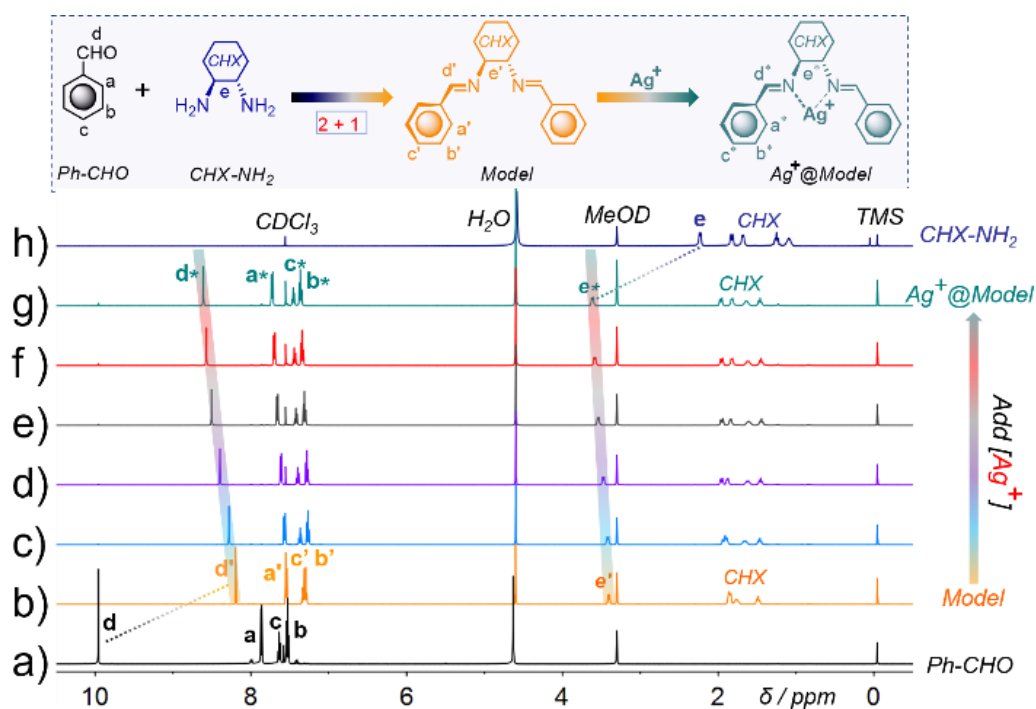


Figure 1. Partial ^1H NMR spectral (400 MHz, 298 K) changes of **Model** in $\text{CDCl}_3/\text{CD}_3\text{OD}$ (v/v, 1/1) in the presence of 0 (b), 0.4 (c), 0.8 (d), 1.2 (e), 1.6 (f), 2.0 (g) equiv. Ag^+ . The ^1H NMR spectra of the precursors **Ph-CHO** (a) and **CHX-NH₂** (h) were given for comparison.

Inferred from the above results, the Schiff-base bidentate **Model** is a potential recognition site for constructing Ag⁺ carriers, thus we chemically modify the **Model** molecule with tetraphenylethylene (TPE) to obtain an Ag⁺ carrier for more entirely store the activity of Ag⁺ through its shielded cavity, and it is likely capable of responsively releasing Ag⁺ and then showing the controllable features. Accordingly, a tetraaldehyde precursor **4-CHO** was synthesized (Scheme S2 and Figures S5-S6) and then condensed with CHX-NH₂ in CDCl₃ in the presence of a catalytic amount of deuterated TFA at 55 °C for 12 h. As depicted in Figure 2b, in this self-assembly system, the characteristic signal of the protons of **4-CHO** completely disappeared, accompanied by the emergence of a set of new ¹H NMR peaks, indicating the production of an enthalpically favored product in high yield (Scheme S3). Based on the experimental findings that two *m/z* signals at 905.4571 [(M + 3H)³⁺] and 679.3442 [(M + 4H)⁴⁺] were discernable in the high-resolution mass spectrum (HRMS) (Figure S7), this large and discrete assembly was tentatively attributed to being a trigonal-prismatic cage, that is, **4-cage**. Its structure was further confirmed by ¹³C NMR, ¹H-¹H NMR COSY, ¹H-¹H NOESY, and 2D diffusion-ordered ¹H NMR spectroscopy (DOSY) characterizations (Figures S8-S12), as well as density functional theory (DFT) calculations (Figure S13). Notably, the signals of H_{a-e} protons in **4-CHO** were observed to upfield shift and split into two sets of signals after assembling into **4-cage**. This might originate from the weaker electron-withdrawing effect of imine than aldehyde, together with the shielded magnetic environment caused by the intimate adjacent TPE units, and/or the non-equivalent spatial environment by the different orientation of the H_{a-e} and H_{a'-e'} protons.

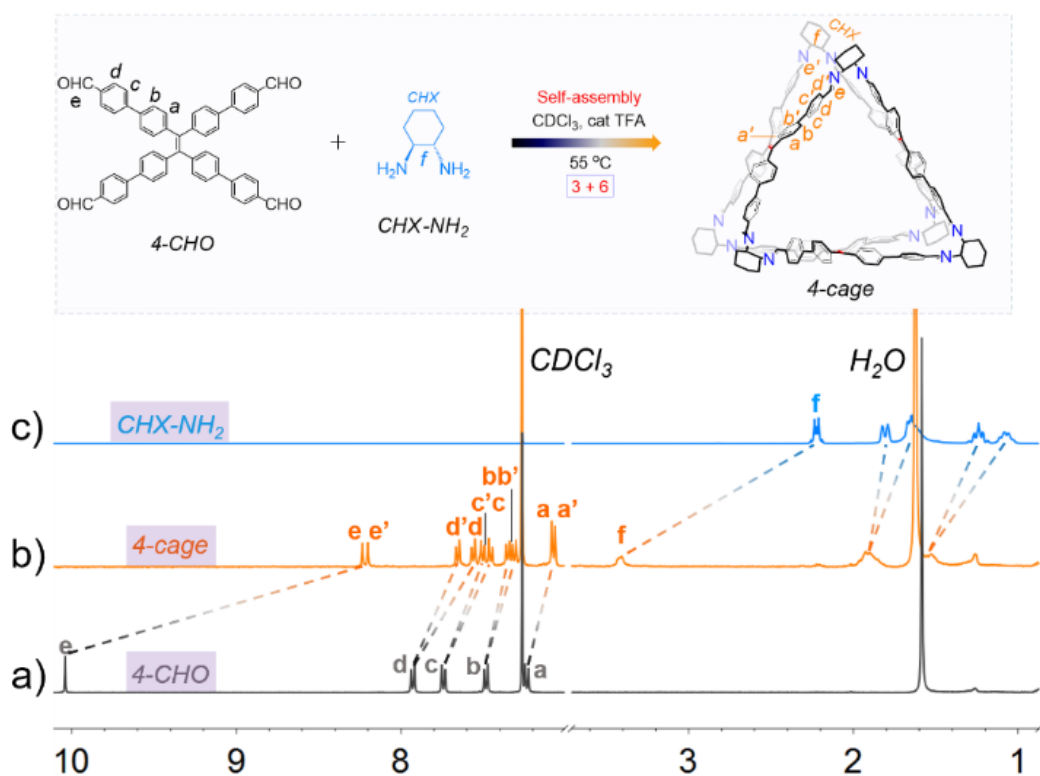


Figure 2. Partial ^1H NMR spectra (500 MHz, CDCl_3 , 298 K) of **4-CHO** (a), **4-cage** (b), and **CHX-NH₂** (c).

After acquiring this cage, we tested the binding case between **4-cage** and Ag^+ ion to deactivate the activity of Ag^+ through coordination. As displayed in Figure 3d-3e, upon addition of Ag^+ ions to the $\text{CDCl}_3/\text{CD}_3\text{OD}$ solution of **4-cage**, we were surprised to observe that all of its ^1H NMR signals disappeared, together with the precipitate produced, suggesting the formation of an intact but insoluble complex (that is, **Ag⁺@4-cage**) through the chelation of imine N atoms with Ag^+ , which is similar to the case of **Model** with Ag^+ . The successful binding of Ag^+ into **4-cage** was also identified by matrix-assisted laser desorption ionization-time of flight (MALDI-TOF) mass spectrometry since the m/z signal with the highest relative abundance appears at 2820.2560, which is assigned to the $[(\mathbf{4-cage} + \text{Ag})^+]$ species (Figure S14). Notably, even with six equiv. of Ag^+ ions added to the solution of **4-cage**, only signals corresponding to the complex with a 1:1 stoichiometric ratio of ligand **4-cage** and Ag^+ could be observed, indicative of the preferential binding pattern is one **4-cage** with one Ag^+ ion. This should be ascribed to the poor solubility of **Ag⁺@4-cage** in the $\text{CHCl}_3/\text{CH}_3\text{OH}$ mixed solution. Evidently, Ag^+ ions should primarily coordinate with electron-rich N atoms due to the presence of lone-pair electrons (see electrostatic potential energy map of **4-cage** in Figure S15). The structure of the **Ag⁺@4-cage**

complex was further confirmed by Fourier transform infrared spectroscopy (FT-IR) and powder X-ray diffraction spectra (P-XRD), where the C=N stretching frequency of **4-cage** shifts from $\sim 1610\text{ cm}^{-1}$ to $\sim 1600\text{ cm}^{-1}$ in the presence of Ag^+ ion (Figure S16), and the peak positions in its P-XRD diffractogram also change significantly (Figure S17), indicating the coordination occurred at imine sites. In addition, DFT calculations reveal the energetically favorable binding of **4-cage** with one Ag^+ via $\text{N}\cdots\text{Ag}$ coordination (see the binding configuration in Figure S18). These results confirmed that this self-assembled **4-cage** supramolecule chemically coordinates with Ag^+ ion rather than physical mixing, while this formed complex precipitates out owing to the poor solubility in $\text{CHCl}_3/\text{CH}_3\text{OH}$ solution.

It is well known that imine bonds are not stable under acidic conditions, which can reversibly recover back to the corresponding reactant aldehyde and amine. Accordingly, the structural disassembly of **4-cage** in its **$\text{Ag}^+@4\text{-cage}$** form may trigger the release of Ag^+ and ultimately achieve the controllable purpose. To evaluate this hypothesis, Ag^+ releasing capabilities of **$\text{Ag}^+@4\text{-cage}$** subject to different equivalents of H^+ ions (0-6 equiv.) were monitored by ^1H NMR titration experiment (Figure 3 and Figure S19). As shown in Figure 3c, after adding H^+ ions to the **$\text{Ag}^+@4\text{-cage}$** -containing mixture, the appearance of 4-CHO NMR signals were observed (Figure 3b), along with the dissolution of the **$\text{Ag}^+@4\text{-cage}$** complex, which indicates that this cage can disassemble under acidic conditions and thereby release Ag^+ .

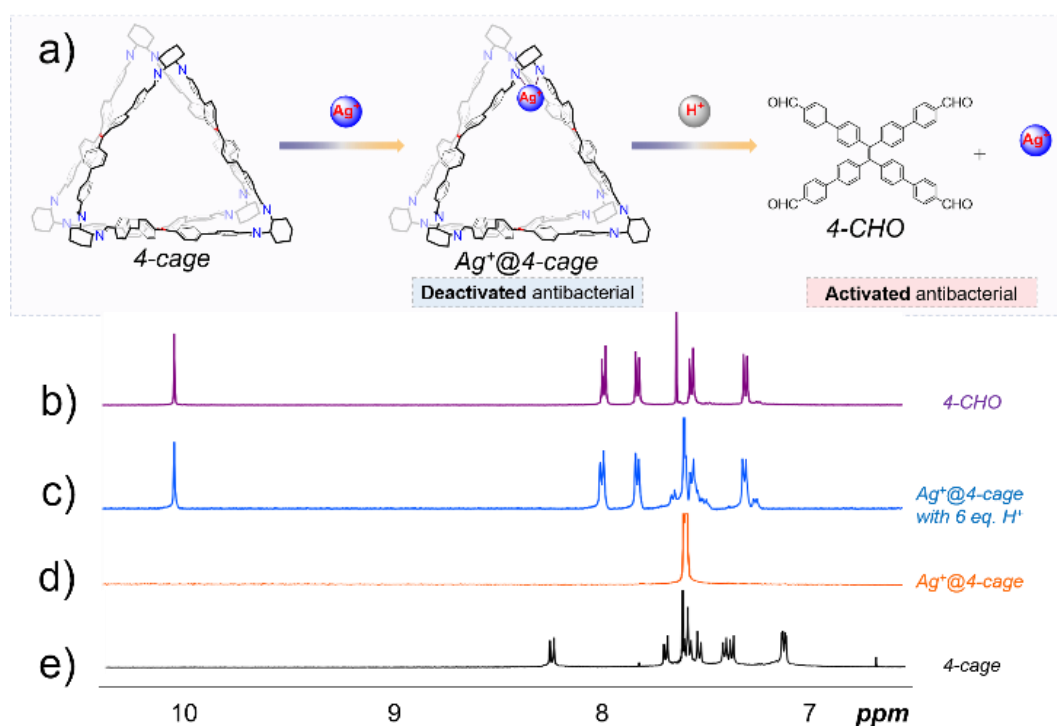


Figure 3. (a) Schematic illustration for the coordination of **4-cage** with Ag^+ , as well as the disassembly in acidic conditions for Ag^+ release. Partial ^1H NMR spectra (500 MHz, 298 K) of **4-CHO** (b), **$\text{Ag}^+@4\text{-cage}$** + 6 equiv. H^+ (c), **4-cage** + Ag^+ (d), **4-cage** (e) in $\text{CDCl}_3/\text{CD}_3\text{OD}$ (v/v, 1/1).

Subsequently, morphology-related experiments were employed to further investigate the influence of Ag^+ and pH towards to **4-cage** on the aggregation of the corresponding species. Dynamic light scattering (DLS) characterization demonstrated that the average size of the **4-cage** sample is 2-3 nm (Figure 4a) and that the resulted sample by adding 6 equiv. of Ag^+ increases sharply to 250-400 nm (Figure 4b), but acid addition triggers these large aggregates to disassemble (Figure 4c). We noted that the average size of the **4-cage** nanoclusters formed after acid addition is ~ 17 nm, which may be attributed to the induced aggregation of the as-resulted species after **4-cage** disassembly. In addition, scanning electron microscope (SEM) was also used to characterize these samples, with the same trend in the sample sizes revealed, that is, no detectable nanoparticle was found for the untreated **4-cage** and the acid-added sample, but nanosphere-like aggregates were observed in the Ag^+ -added sample (Figures 4d-4f).

With all the above characterizations and analysis considered, it can be concluded that the self-assembly **4-cage** indeed coordinates with Ag^+ ion to form **$\text{Ag}^+@4\text{-cage}$** complex thereby deactivating the Ag^+ antibacterial activity, while acid can induce this complex to release the stored- Ag^+ and consequently activate its activity, which may offer the opportunity to employ this Ag^+ -carrying cage for pH-controllable Ag^+ release for antibacterial purposes.

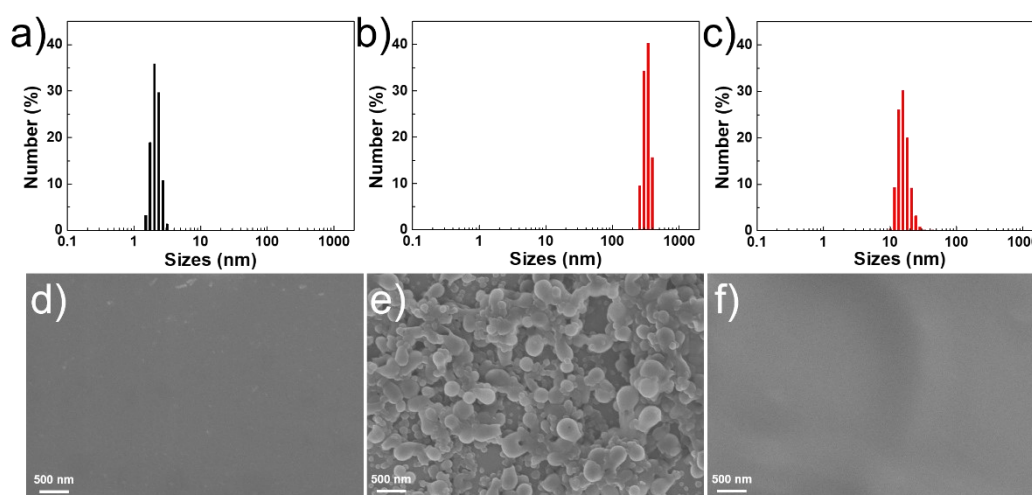


Figure 4. DLS characterization of the **4-cage** sample (a), the **$\text{Ag}^+@4\text{-cage}$** sample (b), and the resulted sample after adding nitric acid to **$\text{Ag}^+@4\text{-cage}$** (c). SEM images of the **4-cage** sample (d), the **$\text{Ag}^+@4\text{-cage}$** sample (e), and the resulted sample after adding nitric acid to **$\text{Ag}^+@4\text{-cage}$** (f).

The antibacterial activity of Ag^+ ions has been applied in many consumer products and medical devices since Ag^+ can interact with thiol and amino groups of proteins and disrupt the protein structure and then efficiently kills microbes including bacteria, fungus, and viruses.^[3] Given that the disassembly of **4-cage** in its **$\text{Ag}^+@4\text{-cage}$** form triggers the release of Ag^+ in acidic conditions, we thus studied the applicability of this Ag^+ -carrying system for bacterial elimination. Gram-negative *Escherichia coli* (*E. coli*, DH5 α strain) was chosen as a model bacterium for the test experiments (Figure 5a). After incubation of the bacterial cells with different concentrations of **4-cage** and **$\text{Ag}^+@4\text{-cage}$** at pH=7.0 (12 h, 30 °C), as indicated by the bacterial colony formation assay (Figure 5b-5c), increasing **$\text{Ag}^+@4\text{-cage}$** concentration was found to decrease the number of alive bacterial cells. By contrast, the empty **4-cage** did not affect the survival of bacterial cells. In addition, the cell cytotoxicity of **4-cage** with or without Ag^+ was measured, and no evident influence on the survival and growth of mammalian cells (MEF and HEK 293T) has been found, indicating the promising non-toxic nature of **4-cage** and **$\text{Ag}^+@4\text{-cage}$** for future biomedical applications (Figure S20).

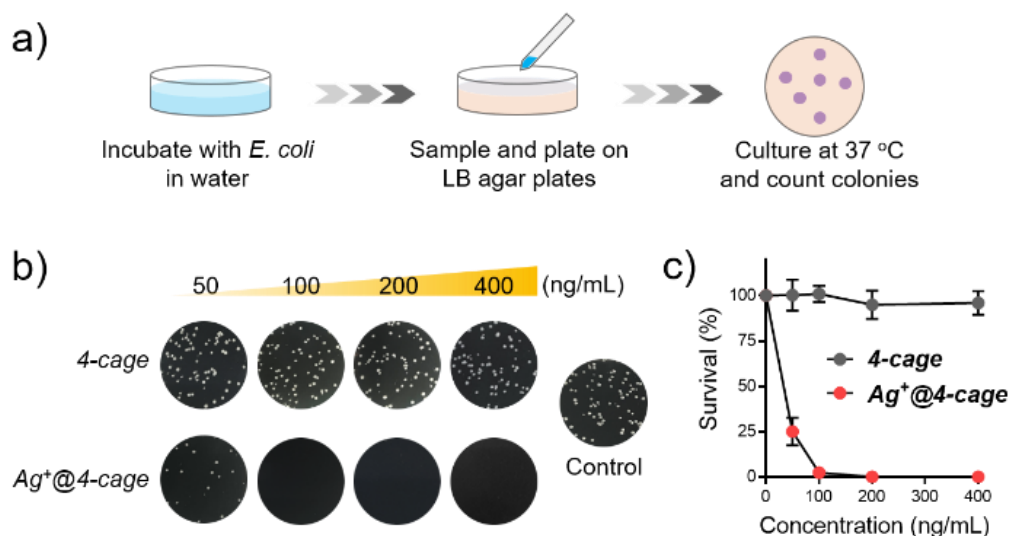


Figure 5. Elimination of *E. coli* by Ag^+ containing **4-cage**. (a) Schematic illustration of the antibacterial test. (b) Photos of *E. coli* colonies after the indicated treatments for 12 h at pH = 7.0. (c) Quantified antibacterial efficacy of **$\text{Ag}^+@4\text{-cage}$** . Data are presented as the mean \pm standard deviation (SD) from three independent experiments.

As discussed above, the release of Ag^+ from the **$\text{Ag}^+@4\text{-cage}$** complex is acid-controllable, we wondered whether lowering the environmental pH promotes its antibacterial efficacy. Firstly, **$\text{Ag}^+@4\text{-cage}$** at a concentration of 25 ng/mL was chosen for verification, which displays no obvious antibacterial efficiency at pH = 7.0 (Figure

6a) but efficiently killed the bacteria when the environmental pH gradually decreases by the adding HNO₃ solution (Figure 6b and Figure S21). A control experiment illustrated that without the presence of **Ag⁺@4-cage**, HNO₃ would not affect the survival of the bacteria; while for the empty cage (Ag⁺-free), even at a concentration of 100 ng/mL, the survival of bacteria was not affected. Secondly, the alive/dead imaging of the bacteria revealed that after adding acid, the release of Ag⁺ from **Ag⁺@4-cage** killed the bacteria in a time-dependent manner (Figure 6c). Although **Ag⁺@4-cage** has no obvious antibacterial activity at lower concentrations and/or neutral conditions, the relatively low pH can significantly enhance the antibacterial efficiency of the **Ag⁺@4-cage** sample by way of releasing Ag⁺ ions. To the best of our knowledge, this is the first example of pH-triggered controllable antibacterial and may be practically applied to eliminate bacteria in specific acidic microenvironments.

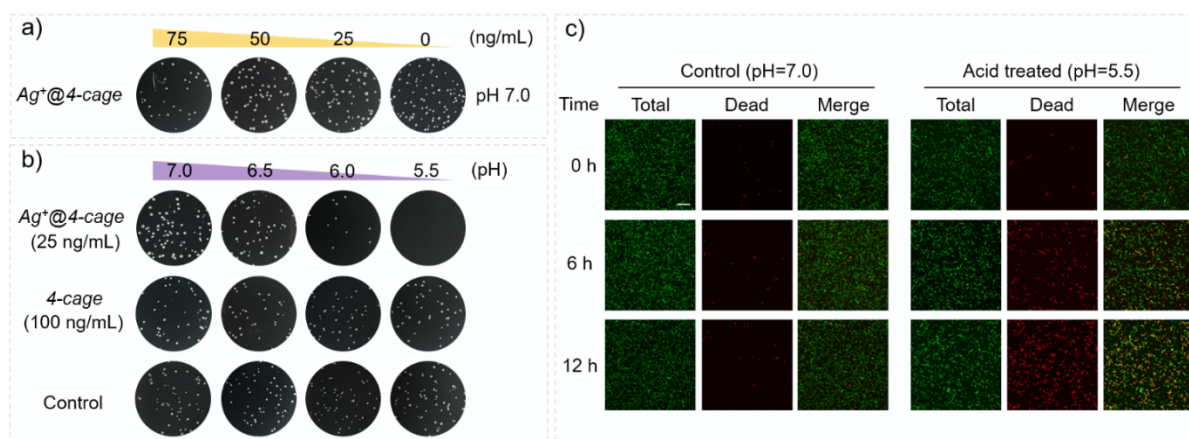


Figure 6. Acid triggered release of Ag⁺ for antibacterial treatment. (a) Photos of *E. coli* colonies after treatment with different concentrations of **Ag⁺@4-cage** for 12 h at pH = 7.0. (b) Photos of *E. coli* colonies after treatment at different pH for 12 h. (c) Alive/dead imaging of bacteria during acid-triggered Ag⁺ release. The *E. coli* cells expressing green fluorescent protein were incubated with 10 μM propidium iodide to show the dead bacteria with compromised membrane permeability. Scale bar represents 10 μm.

3 Conclusion

In summary, by using imine chemistry, we proposed a molecular design strategy for constructing an Ag⁺-containable pure organic molecular cage that is capable of responsively releasing Ag⁺ at acidic environments to realize pH-triggered controllable bacterial elimination. This self-assembly supramolecular architecture bears dynamic reversible imine subunits as chelating sites coordinating with Ag⁺ to deactivate its antibacterial activity, whereas specific acid conditions break the imine bonds and disassemble this cage triggering Ag⁺ release to achieve and activate its controllable antibacterial properties. Such a responsive bacteria-killing strategy through molecular self-assembly not only provides reference to develop novel approaches for targeted

antibacterial applications at specific pH conditions but also offers the opportunity for scientists to design relevant types of novel materials with controllable functions in various other fields.

Conflict of interest

The authors declare no competing financial interest.

Acknowledgement

This work was financial support from the National Natural Science Foundation of China (12004209) and the Colleges and Universities Twenty Terms Foundation of Jinan City (2019GXRC034).

4 References

- (1) Woese, C. R., Bacterial evolution. *Microbiol. Rev.* **1987**, *51*, 221-271.
- (2) Silver, L. L., Challenges of antibacterial discovery. *Clin Microbiol Rev* **2011**, *24*, 71-109.
- (3) Chernousova, S.; Epple, M., Silver as antibacterial agent: ion, nanoparticle, and metal. *Angew. Chem., Int. Ed.* **2013**, *52*, 1636-1653.
- (4) Eckhardt, S.; Brunetto, P. S.; Gagnon, J.; Priebe, M.; Giese, B.; Fromm, K. M., Nanobio silver: its interactions with peptides and bacteria, and its uses in medicine. *Chem. Rev.* **2013**, *113*, 4708-4754.
- (5) Richter, A. P.; Brown, J. S.; Bharti, B.; Wang, A.; Gangwal, S.; Houck, K.; Cohen Hubal, E. A.; Paunov, V. N.; Stoyanov, S. D.; Velev, O. D., An environmentally benign antimicrobial nanoparticle based on a silver-infused lignin core. *Nat. Nanotechnol.* **2015**, *10*, 817-823.
- (6) Xu, Z.; Zhang, C.; Wang, X.; Liu, D., Release strategies of silver ions from materials for bacterial killing. *ACS Appl. Bio Mater.* **2021**, *4*, 3985-3999.
- (7) Jin, Y.; Voss, B. A.; Jin, A.; Long, H.; Noble, R. D.; Zhang, W., Highly CO₂-selective organic molecular cages: what determines the CO₂ selectivity. *J. Am. Chem. Soc.* **2011**, *133*, 6650-6658.

- (8) Jin, Y.; Voss, B. A.; Noble, R. D.; Zhang, W., A shape-persistent organic molecular cage with high selectivity for the adsorption of CO₂ over N₂. *Angew. Chem., Int. Ed.* **2010**, *49*, 6348-6351.
- (9) Wang, L.; Cheng, L.; Li, G.; Liu, K.; Zhang, Z.; Li, P.; Dong, S.; Yu, W.; Huang, F.; Yan, X., A self-cross-linking supramolecular polymer network enabled by crown-ether-based molecular recognition. *J. Am. Chem. Soc.* **2020**, *142*, 2051-2058.
- (10) Yang, X.; Sun, J.-K.; Kitta, M.; Pang, H.; Xu, Q., Encapsulating highly catalytically active metal nanoclusters inside porous organic cages. *Nat. Catal.* **2018**, *1*, 214-220.
- (11) Wang, Y.; Sun, Y.; Shi, P.; Sartin, M. M.; Lin, X.; Zhang, P.; Fang, H.; Peng, P.; Tian, Z.; Cao, X., Chaperone-like chiral cages for catalyzing enantio-selective supramolecular polymerization. *Chem. Sci.* **2019**, *10*, 8076-8082.
- (12) Zhang, M.; Saha, M. L.; Wang, M.; Zhou, Z.; Song, B.; Lu, C.; Yan, X.; Li, X.; Huang, F.; Yin, S.; Stang, P. J., Multicomponent platinum(II) cages with tunable emission and amino acid sensing. *J. Am. Chem. Soc.* **2017**, *139*, 5067-5074.
- (13) Zheng, X.; Zhu, W.; Zhang, C.; Zhang, Y.; Zhong, C.; Li, H.; Xie, G.; Wang, X.; Yang, C., Self-assembly of a highly emissive pure organic imine-based stack for electroluminescence and cell imaging. *J. Am. Chem. Soc.* **2019**, *141*, 4704-4710.
- (14) Yu, G.; Cook, T. R.; Li, Y.; Yan, X.; Wu, D.; Shao, L.; Shen, J.; Tang, G.; Huang, F.; Chen, X.; Stang, P. J., Tetraphenylethene-based highly emissive metallacage as a component of theranostic supramolecular nanoparticles. *Proc. Natl. Acad. Sci. USA* **2016**, *113*, 13720-13725.
- (15) Saha, M. L.; Yan, X.; Stang, P. J., Photophysical properties of organoplatinum(II) compounds and derived self-assembled metallacycles and metallacages: fluorescence and its applications. *Acc. Chem. Res.* **2016**, *49*, 2527-2539.
- (16) Sun, Y.; Chen, C.; Stang, P. J., Soft materials with diverse suprastructures via the self-assembly of metal-organic complexes. *Acc. Chem. Res.* **2019**, *52*, 802-817.
- (17) Rizzuto, F. J.; von Krbek, L. K. S.; Nitschke, J. R., Strategies for binding multiple guests in metal-organic cages. *Nat. Rev. Chem.* **2019**, *3*, 204-222.
- (18) Roberts, D. A.; Pilgrim, B. S.; Nitschke, J. R., Covalent post-assembly modification in metallosupramolecular chemistry. *Chem. Soc. Rev.* **2018**, *47*, 626-644.
- (19) Acharyya, K.; Mukherjee, P. S., Organic imine cages: molecular marriage and applications. *Angew. Chem., Int. Ed.* **2019**, *58*, 8640-8653.

- (20) Liu, K.; Liu, Y.; Yao, Y.; Yuan, H.; Wang, S.; Wang, Z.; Zhang, X., Supramolecular photosensitizers with enhanced antibacterial efficiency. *Angew. Chem., Int. Ed.* **2013**, *52*, 8285-8289.
- (21) Ma, X.; Zhao, Y., Biomedical applications of supramolecular systems based on host-guest interactions. *Chem. Rev.* **2015**, *115*, 7794-839.
- (22) Hu, B.; Owh, C.; Chee, P. L.; Leow, W. R.; Liu, X.; Wu, Y. L.; Guo, P.; Loh, X. J.; Chen, X., Supramolecular hydrogels for antimicrobial therapy. *Chem. Soc. Rev.* **2018**, *47*, 6917-6929.
- (23) Wang, H.; Qian, X.; Wang, K.; Su, M.; Haoyang, W. W.; Jiang, X.; Brzozowski, R.; Wang, M.; Gao, X.; Li, Y.; Xu, B.; Eswara, P.; Hao, X. Q.; Gong, W.; Hou, J. L.; Cai, J.; Li, X., Supramolecular Kandinsky circles with high antibacterial activity. *Nat. Commun.* **2018**, *9*, 1815.
- (24) Yang, Y.; He, P.; Wang, Y.; Bai, H.; Wang, S.; Xu, J. F.; Zhang, X., Supramolecular radical anions triggered by bacteria in situ for selective photothermal therapy. *Angew. Chem., Int. Ed.* **2017**, *56*, 16239-16242.
- (25) Li, X.; Bai, H.; Yang, Y.; Yoon, J.; Wang, S.; Zhang, X., Supramolecular antibacterial materials for combatting antibiotic resistance. *Adv. Mater.* **2019**, *31*, e1805092.
- (26) Xie, X.; Sun, T.; Xue, J.; Miao, Z.; Yan, X.; Fang, W.; Li, Q.; Tang, R.; Lu, Y.; Tang, L.; Zha, Z.; He, T., Ag nanoparticles cluster with pH-triggered reassembly in targeting antimicrobial applications. *Adv. Funct. Mater.* **2020**, *30*, 2000511.
- (27) Nejman, D.; Livyatan, I.; Fuks, G.; Gavert, N.; Zwang, Y.; Geller, L. T.; Rotter-Maskowitz, A.; Weiser, R.; Mallel, G.; Gigi, E.; Meltser, A.; Douglas, G. M.; Kamer, I.; Gopalakrishnan, V.; Dadosh, T.; Levin-Zaidman, S.; Avnet, S.; Atlan, T.; Cooper, Z. A.; Arora, R.; Cogdill, A. P.; Khan, M. A. W.; Ologun, G.; Bussi, Y.; Weinberger, A.; Lotan-Pompan, M.; Golani, O.; Perry, G.; Rokah, M.; Bahar-Shany, K.; Rozeman, E. A.; Blank, C. U.; Ronai, A.; Shaoul, R.; Amit, A.; Dorfman, T.; Kremer, R.; Cohen, Z. R.; Harnof, S.; Siegal, T.; Yehuda-Shnaidman, E.; Gal-Yam, E. N.; Shapira, H.; Baldini, N.; Langille, M. G. I.; Ben-Nun, A.; Kaufman, B.; Nissan, A.; Golan, T.; Dadiani, M.; Levanon, K.; Bar, J.; Yust-Katz, S.; Barshack, I.; Peeper, D. S.; Raz, D. J.; Segal, E.; Wargo, J. A.; Sandbank, J.; Shental, N.; Straussman, R., The human tumor microbiome is composed of tumor type-specific intracellular bacteria. *Science* **2020**, *368*, 973-980.
- (28) Fan, Y.; Pedersen, O., Gut microbiota in human metabolic health and disease. *Nat Rev Microbiol* **2021**, *19*, 55-71.

(29) Aranda-Diaz, A.; Obadia, B.; Dodge, R.; Thomsen, T.; Hallberg, Z. F.; Guvener, Z. T.; Ludington, W. B.; Huang, K. C., Bacterial interspecies interactions modulate pH-mediated antibiotic tolerance. *Elife* **2020**, *9*, e51493.